AIAA JOURNAL
Vol. 33, No. 11, November 1995

Buffeting of Fin: Distortion of Incident Vortex

S. Canbazoglu,* J.-C. Lin,† S. Wolfe,† and D. Rockwell‡
Lehigh University, Bethlehem, Pennsylvania 18015

The encounter of a broken-down vortex with the swept leading edge of a fin is investigated in a water channel using high-image-density particle image velocimetry, which leads to instantaneous fields of velocity and vorticity. The vortex-fin interaction generates a layer of time-averaged vorticity extending along the entire leading edge from the root to the tip of the fin. This averaged vorticity is actually due to a succession of instantaneous states of highly concentrated vorticity along the edge of the postbreakdown region of the vortex. Above the surface of the fin, however, the averaged vorticity has a relatively low level; the corresponding instantaneous vorticity concentrations have alternating sign and are not repetitive in space or time. Nevertheless, two-dimensional correlations of instantaneous vorticity exhibit well-defined peaks corresponding to an identifiable wavelength between the vorticity concentrations. Spectra of surface pressure at crucial locations on the fin are related to these features of the instantaneous and averaged flow structure.

Nomenclature

C = chord of delta wing
C_F = root chord of fin
f = frequency
M = magnification
R_ω = vorticity correlation function
t = thickness of wing, time
t_F = thickness of fin
U = freestream velocity
x = coordinate along axis of vortex
y = coordinate in plane of fin
z = coordinate perpendicular to surface of fin
α = angle of attack of delta wing
Δ = distance from plane of fin to plane of laser sheet
Δt = sampling time
Δ^* $\equiv \Delta/C_F$, distance from plane of fin to plane of laser sheet normalized by root chord of fin
η = variable along y axis
Λ = sweep angle of wing, deg
Λ_F = sweep angle of fin
λ_v = sweep angle of axis of leading-edge vortex
ν = kinematic viscosity
ξ = variable along x axis
ω_z = vorticity component orthogonal to plane of fin
$\tilde{\omega}$ = vorticity fluctuation
$\bar{\omega}$ = time-averaged vorticity
$\langle\rangle_{sp}$ = spatial average over entire plane of observation

I. Introduction

In recent years, buffeting of aircraft fins and tails has become an issue of central interest. A wide variety of investigations have addressed the buffet-induced loading on models of actual aircraft. Triplett[1] measured the unsteady surface pressure on the surface of a rigid tail of an F-15. In a series of investigations, Lee et al.,[2] Brown et al.,[3] Lee and Tang,[4] Lee and Brown,[5] and Lee et al.[6] measured the surface pressure and unsteady forces on the surface of a fin and over the cross section of its wake for F/A-18 and CF-18 aircraft configurations. Ferman et al.,[7] Shah,[8] Shah et al.,[9] and Patel[9] also provide insight into the unsteady surface loading of fins on the F/A-18 and F-18 models. Bean and Wood[10] and Washburn et al.[11] characterize the loading on a fin located upstream and downstream of the trailing edge of a delta wing, respectively. An important feature of all of the foregoing studies, extending over relatively wide ranges of Reynolds and Mach numbers, is the occurrence of a generally well-defined peak in the spectra of the surface pressure. Although these spectra exhibit, to varying degrees, a broad distribution of energy about the peak, the existence of such an identifiable frequency, or at least a defined band of frequencies, suggests that the broken-down vortex incident upon the fin exhibits a degree of coherence.

Relatively little is known of the fluctuating flowfield adjacent to the surface of the fin that gives rise to the unsteady surface pressure. Lee et al.[12] and Hebbar et al.[13] provide distributions of the averaged rms velocity fluctuations adjacent to the fin of an F/A-18 and YF-17. Similarly, LeMay and Lovato[14] characterize the turbulent fluctuations in the vicinity of an F-15 fin. These features of the fluctuating velocity field adjacent to the fin are complemented by averaged surface flow patterns obtained by oil streak techniques in the investigations of Lee et al.,[2] Brown et al.,[3] Lee and Tang,[4] and Washburn et al.[11] Such patterns allow identification of the extent of regions of separated unsteady and attached flow, as well as the general direction of the surface flow, which often can exhibit a pronounced component in the upper direction toward the tip of the fin.

The objective of the present investigation is to characterize the incident vortex-fin interaction for the simplified configuration of a delta wing. Emphasis is on the quantitative, instantaneous structure of the flow pattern over the entire surface of the fin in relation to the incident, broken-down vortex. In turn, the averaged flow structure is determined from a sequence of instantaneous states. This approach is in the spirit of the recent investigation of Mayori and Rockwell,[15] which addresses the simplified configuration of a broken-down vortex incident upon a rectangular plate located downstream of the trailing edge of a delta wing, in contrast to the present configuration of a swept leading-edge fin on the surface of the wing. Various combinations of instantaneous and averaged velocity fields, streamline patterns, and vorticity contours, in conjunction with root-mean-square representations of vorticity fluctuations and instantaneous vorticity correlations, provide a rational basis for the corresponding pressure spectra, which are measured at crucial locations on the surface of the fin.

II. Experimental System and Techniques

All experiments were performed at a flow velocity of 147 mm/s in a water channel having a cross section of 616 × 584 mm. As indicated in Fig. 1, a delta wing having a sweep angle of 75 deg was employed. It had a chord of 330 mm and a thickness to chord ratio $t_w/C = 0.0192$. The windward side of the wing was beveled at an

Received Aug. 27, 1994; revision received Jan. 20, 1995; accepted for publication Jan. 27, 1995.

*On leave from Erciyes University, Müh. Fak. Makina Müh., Bölümü, 38090 Kocasinan/Kayseri, Turkey.
†Research Associate, Department of Mechanical Engineering and Mechanics.
‡Paul B. Reinhold Professor, Department of Mechanical Engineering and Mechanics. Member AIAA.

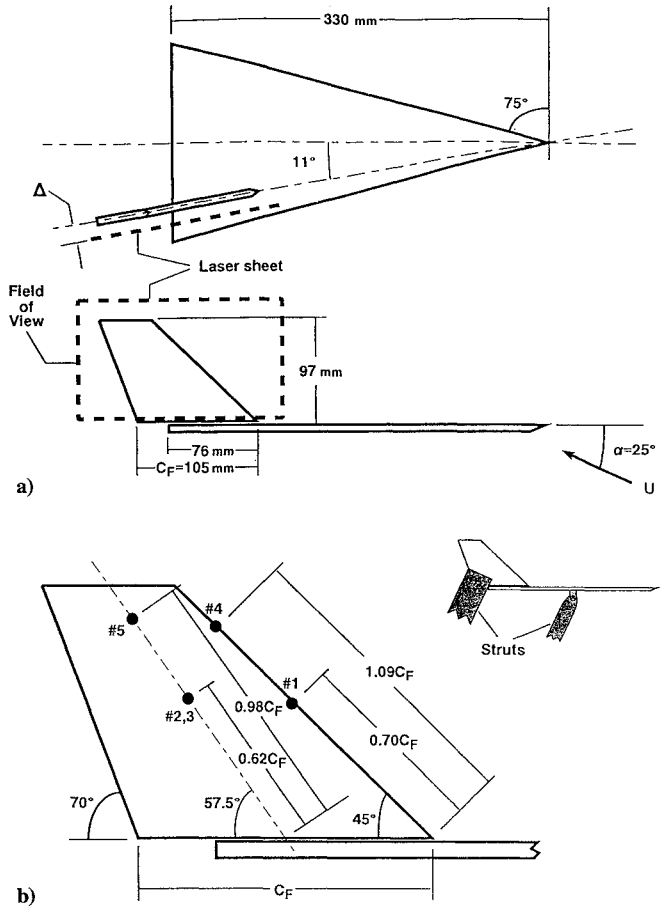

Fig. 1 Overview of delta wing-fin system.

angle of 30 deg. The Reynolds number based on chord C was $Re = UC/\nu = 4.86 \times 10^4$. A rigid fin was mounted in line with the axis of the leading-edge vortex, at an effective sweep angle $\Lambda_v \cong 79$ deg. This fin had a thickness to chord ratio $t_F/C_F = 0.12$. The leading edge and tip of the fin were double beveled at an angle of 30 deg. The location of pressure taps on the surface of the fin are indicated in Fig. 1b, where each dimension is expressed as a coefficient of the root chord of the fin C_F. Taps 1 and 4 are at the tip of the leading edge, taps 2 and 5 on the outboard surface, and tap 3 on the inboard surface of the fin. The delta wing was held in position using a traditional streamlined strut at its midchord. The fin was supported by a thin vertical strut connected to the fin at its trailing corner adjacent to the trailing edge of the wing; the strut thickness was $t/C_F = 0.12$. To facilitate laser diagnostics, the fin–delta wing assembly was actually inverted in the water channel, as indicated in Fig. 1. Emphasis was on an angle of attack $\alpha = 25$ deg for which the location of vortex breakdown is just upstream of the leading edge of the fin. At higher values of α, where breakdown occurs farther upstream of the fin, the flow structure and surface pressure loading on the fin will be altered accordingly. Proper normalization, however, leads to general similarities of previous related investigations over a range of α, as assessed by Wolfe et al.[20]

To determine the instantaneous flow structure over an entire plane, a laser scanning version of high-image-density particle image velocimetry (PIV) was employed. This technique is described by Rockwell et al.,[16] Rockwell et al.,[17] and Rockwell and Lin.[18] A rapidly scanning laser sheet illuminated metallic-coated particles having a diameter of 12 μm, providing the field of view indicated in Fig. 1a. The laser sheet was displaced from the centerplane of the fin a distance Δ^*. This scanning sheet originated from a continuous wavelength argon-ion laser (3 W), was transmitted through a series of conditioning optics, and impinged upon a rotating mirror having 72 facets, providing an effective scanning frequency of 500 Hz. Multiply exposed images were acquired using a Nikon F-4 camera, having a 105-mm lens with a magnification $M = 0.1645$. The patterns of particle images on the 35-mm high-resolution Tmax Kodak film (400 ASA) were interrogated with a high-resolution Nikon digitizer system at 125 pixels/mm. A single-frame cross-correlation technique was employed to determine the velocity field. Approximately 3400 velocity vectors were determined for each image. On the plane of the negative, the dimensions of the interrogation window during velocity calculation were 0.8 × 0.8 mm or, in the physical plane of the laser sheet, 4.86 × 4.86 mm. During the evaluation process, the image was interrogated with a 50% overlap in order to satisfy the Nyquist criterion, thereby providing an effective grid size $\Delta\ell/M = 2.43$ mm in the plane of the laser sheet. This grid size corresponds to 1.22% of the total length of the images shown herein. During processing of the velocity field, a Gaussian filter with a factor $p = 1.3$ is applied. No additional filtering of the data was carried out. The instantaneous velocity field obtained in this manner allowed calculation of the corresponding instantaneous contours of constant vorticity, as well as sectional streamline patterns. The actual acquisition time for each instantaneous image was of the order of 10 ms. Averaged representations were constructed from averaging a total of 20 instantaneous images, acquired at a large time spacing, corresponding to $5C/U$ where C/U is the convective timescale. This time spacing is much longer than the predominant period of the pressure fluctuations induced by the vortex breakdown, thereby ensuring random sampling.

Pressure measurements were performed at the locations indicated in Fig. 1b. Each pressure tap was connected to a 1.59-mm transmission line fabricated within the interior of the streamline support 203 mm extending from the trailing bottom corner of the fin to a location above the free surface of the water channel. At this location above the free surface, all transducers were mounted in a block of Plexiglas®. All pressure data were acquired using five Piezotronics 106B50 transducers with a 480D06 power unit, a Tektronix amplifier and a Kronhite filter set to allow low pass below a cutoff frequency of 10 Hz.

The transducer-transmission line system was determined to have a resonant frequency of 8.33 Hz. Examination of the transient response characteristics revealed that the amplitude distortion and phase shift were 2.1% and 0.015 rad, respectively, at the primary frequencies of interest in this investigation.

The spectrum of the pressure fluctuations was determined by first digitizing the signal at the sampling rate $\Delta t = 0.05$ s. Each of these digitized records corresponded to approximately 61 cycles of the predominant frequency of the pressure fluctuation. To determine the averaged spectrum, a total of 15 continuous records of length 1024 points were acquired. Then, each of these records was segmented into 2 subrecords in order to calculate the final averaged spectrum.

III. Instantaneous and Averaged Flow Structure

The vortex distortion past in the fin is described in terms of averaged patterns of streamlines and vorticity contours, as well as instantaneous vorticity contours. First, the averaged state of the flow is addressed; it provides a framework for interpreting the instantaneous distortion mechanisms along the leading edge and surface of the fin.

A. Overview of Averaged Flow: Velocity Fields

Figure 2 shows the averaged velocity field on a plane intersecting the leading edge of the fin, i.e., $\Delta^* = \Delta/C_F = 0$, as well as on planes at increasing distance Δ^* from the fin. The bold vector at the top right corner of the image corresponding to $\Delta^* = 0$ represents the magnitude of the freestream velocity. On the plane $\Delta^* = 0$, the onset of vortex breakdown, marked by the abrupt onset of a large-scale, low-velocity zone of separation, is evident in the lower right portion of the image. As this broken-down vortex encounters the leading edge of the fin, it is deflected in a manner such that its outer edge takes the form of a mixing layer type flow, bounded at the other extreme by the solid boundary corresponding to the leading edge of the fin. At $\Delta^* = 0.06$, this mixing layer drives a large-scale recirculating flow, corresponding to the existence of large-scale separation along the surface of the fin. A region of relatively low velocity is located on the outer part of the fin near the tip. At $\Delta^* = 0.12$, the general form of this recirculating zone persists,

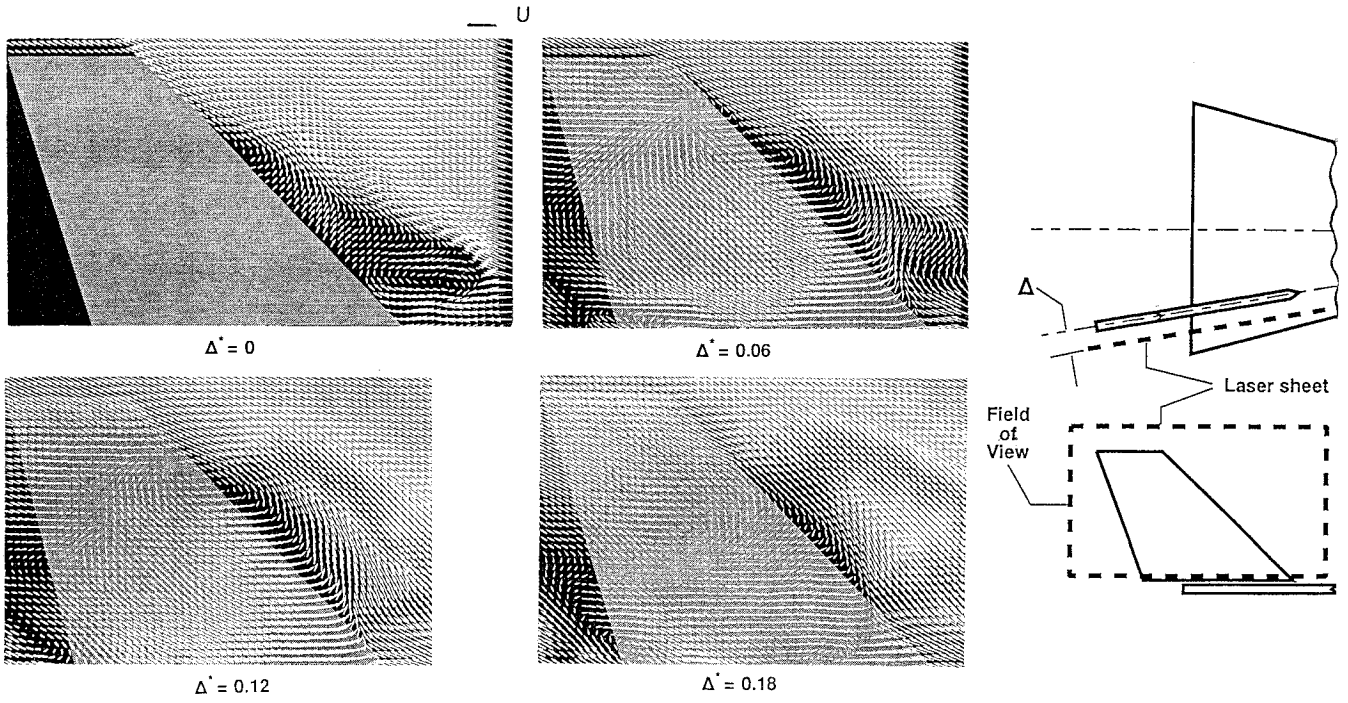

Fig. 2 Averaged velocity fields at various distances from surface of fin, uncertainty of averaged velocity is 0.2%.

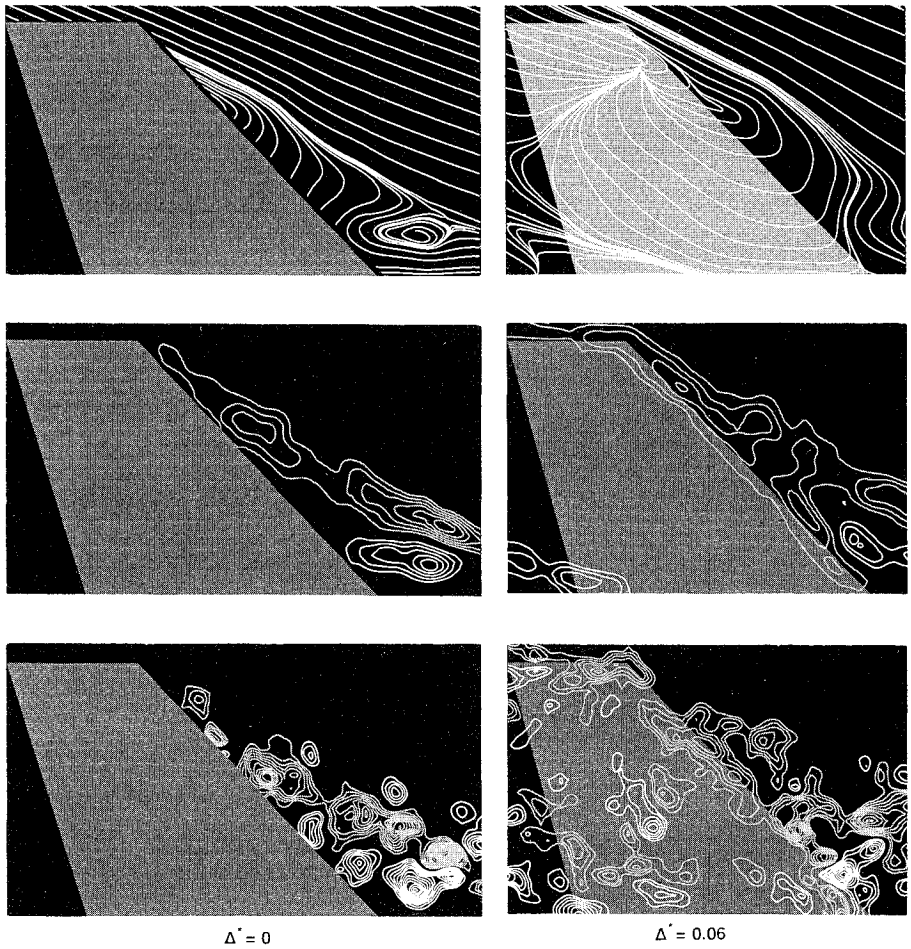

Fig. 3a Averaged streamline patterns (top row), contours of constant vorticity (middle row), and instantaneous vorticity contours (bottom row) as a function of dimensionless distance Δ^* from surface of fin. For averaged and instantaneous vorticity contours, minimum and incremental levels of vorticity are ± 5 1/s and 3 1/s, respectively. Uncertainty of vorticity in this and subsequent figures is 6%.

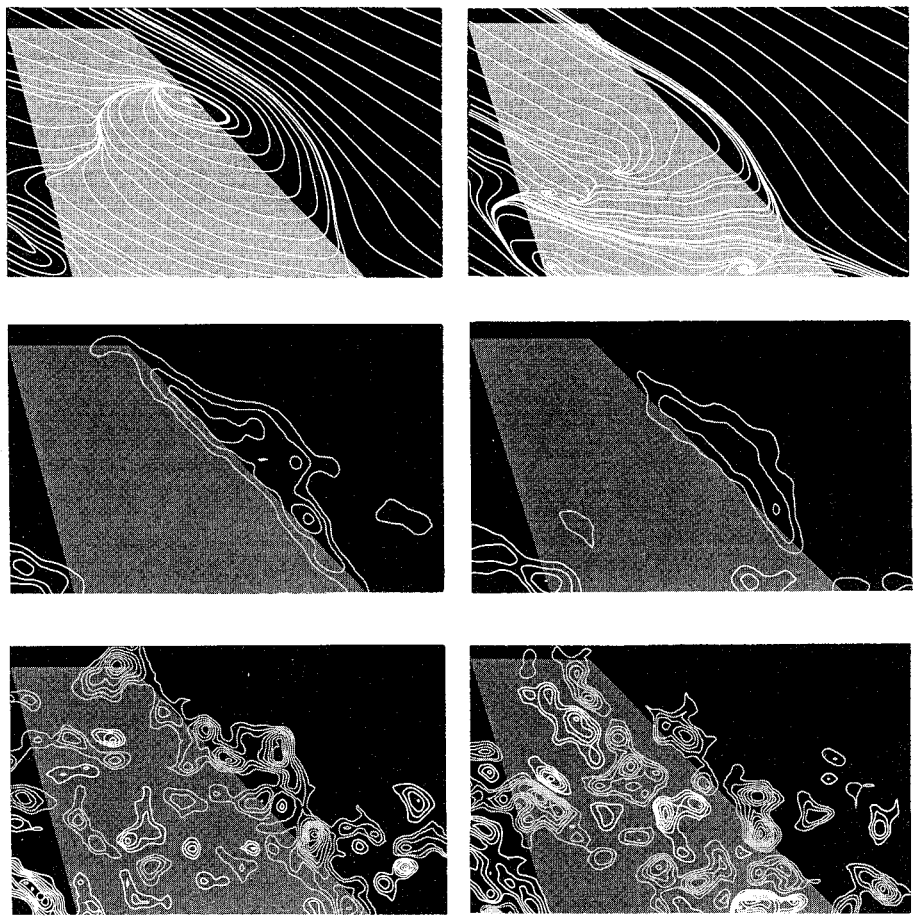

Fig. 3b Averaged streamline patterns (top row), contours of constant vorticity (middle row), and instantaneous vorticity contours (bottom row) as a function of dimensionless distance Δ^* from surface of fin; for averaged and instantaneous vorticity contours, minimum and incremental levels of vorticity are ±5 1/s and 3 1/s, respectively.

and at $\Delta^* = 0.18$, the low-velocity region has migrated toward the root of the fin. These patterns suggest that there is a region of large-scale separated flow on this outboard side of the fin. Large-scale separation extending over nearly the entire outboard region of the fin of an F/A-18 aircraft is described by Lee and Tang,[4] in conjunction with the qualitative flow visualization of Fisher et al.[19] Moreover, the surface visualization of Washburn et al.[11] shows complex patterns of surface flow on the outboard side of the fin, in contrast to those on the inboard side where the flow is generally aligned in the chordwise direction.

B. Comparison of Averaged and Instantaneous Structure

Direct comparison of the averaged streamlined patterns, corresponding to the averaged velocity fields of Fig. 2, averaged contours of vorticity ω_z orthogonal to the plane of the fin, and instantaneous contours of ω_z are given in Figs. 3a and 3b for increasing spanwise displacement Δ^* of the plane observation relative to the plane of the fin.

For $\Delta/C_F = \Delta^* = 0$, the averaged streamline pattern clearly shows the boundary between the freestream and the mixing layer, as well as the entrainment streamlines extending from a region near the leading edge. The corresponding contours of averaged vorticity show that positive (white) vorticity is confined to the region immediately downstream of vortex breakdown, whereas negative (gray) vorticity extends all of the way from the onset of breakdown to the tip of the fin. These averaged representations of vorticity are, however, due to a sequence of instantaneous states of the sort shown in the bottom image at $\Delta^* = 0$. Onset of instantaneous vortex breakdown, occurring at the bottom-right portion of the image, is marked by switching of the concentration of positive vorticity from the location well away from the surface of the wing to a position close to the surface and, conversely, for the negative concentration of vorticity. The helical mode instability of the breakdown is suggested by the alternating street of positive and negative concentrations of vorticity; smaller concentrations of positive vorticity are due to helical type instabilities about the exterior of the broken-down vortex. Sufficiently far downstream of breakdown, only negative concentrations of instantaneous vorticity are evident, in accord with the general trend of the averaged vorticity pattern.

At $\Delta^* = 0.06$, the averaged streamline pattern shows a nodal line, above which the streamlines move toward the tip of the fin, and below it toward the root of the fin. This nodal line is consistent with the recirculation zone approximately centered along the leading edge of the fin. Corresponding contours of averaged vorticity shown maxima close to the leading edge of the fin; moreover, this vorticity layer extends not only along the leading edge, but also along the tip region of the fin. A representative pattern of instantaneous concentrations of vorticity, shown at the bottom of the series $\Delta^* = 0.06$, indicates that pronounced concentrations of only negative vorticity dominate the leading edge and tip regions of the fin. Along the surface of the fin, vorticity reorientation and stretching has apparently given rise to both positive and negative concentrations of vorticity; they generally have a lower level than those along the leading edge and tip.

At a larger value of $\Delta^* = 0.12$, shown in Fig. 3b, the general form of the streamline pattern is in the form of an unstable limit cycle, approximately centered on the leading edge of the fin. Within this limit cycle, the streamline pattern spirals inward and, exterior to it, the streamline spirals outward. The averaged and instantaneous vorticity distributions exhibit the same general features as those at $\Delta^* = 0.06$.

Finally, at the largest value of $\Delta^* = 0.18$, the streamline pattern again tends to the form of a nodal line, which has shifted toward the root of the fin. The extent of the averaged vorticity contours is

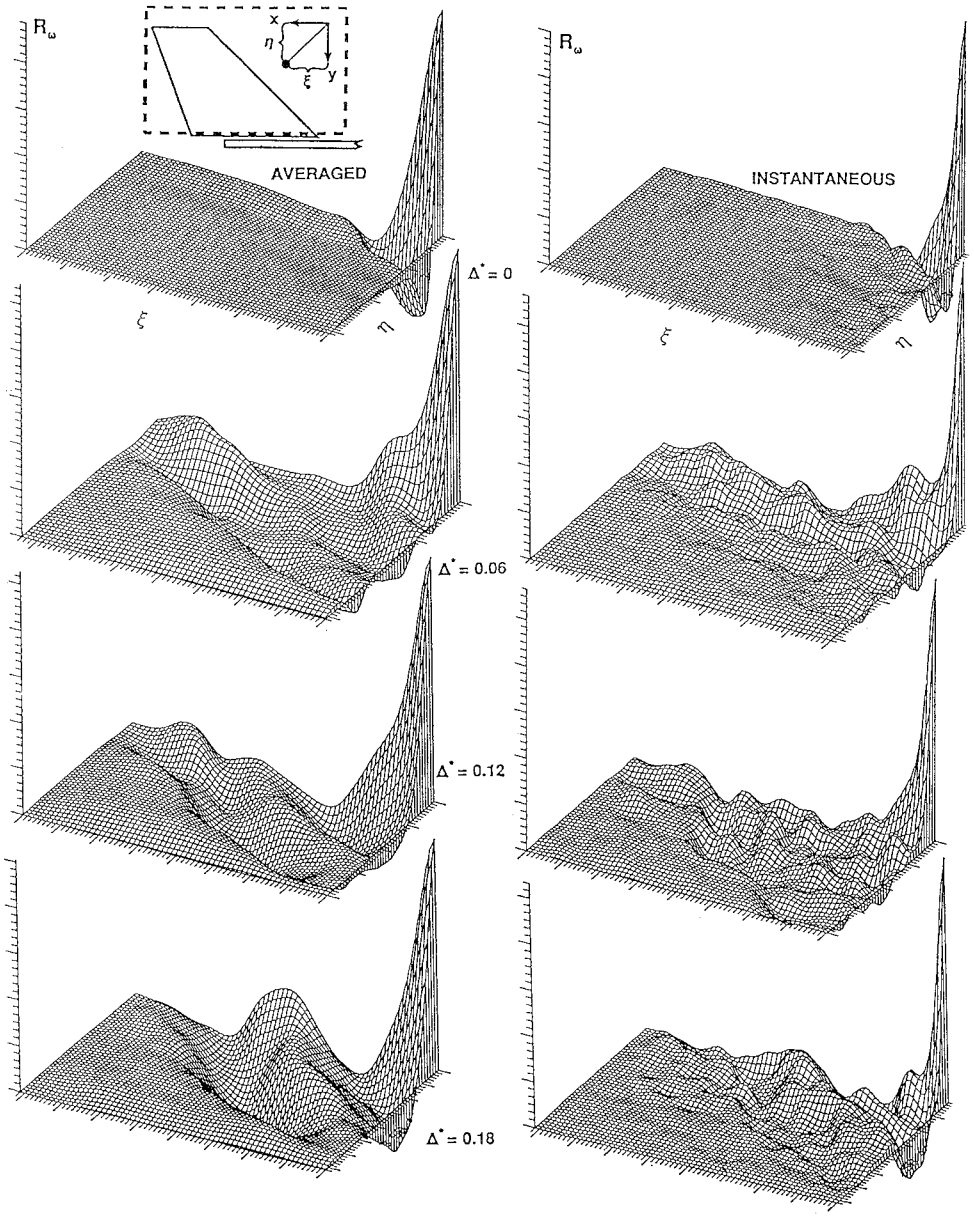

Fig. 4 Three-dimensional plots showing vorticity correlation R_ω as a function of separation distance ξ and η; averaged R_ω (left column) obtained from averaged vorticity distributions; instantaneous R_ω (right column) calculated from corresponding instantaneous vorticity distributions of Fig. 3.

confined to the midregion of the leading edge. Instantaneous concentrations of vorticity, shown in the bottom image of the series, again show pronounced negative concentrations on the leading-edge and tip regions. Over the surface of the fin, however, both positive and negative concentrations of substantial level are observed.

IV. Vorticity Correlations

To obtain a quantitative representation of the distribution of scales of vortical structures of the averaged and instantaneous vorticity plots of Fig. 3, the two-dimensional vorticity correlation function R_ω is employed. It is defined as

$$R_\omega = \frac{\langle \omega_z(x, y)\omega_z(x + \xi, y + \eta)\rangle_{sp}}{\omega^2_{rms}} \qquad (1)$$

Plots of the vorticity correlation R_ω, corresponding to the averaged vorticity fields of Figs. 3a and 3b, are shown in the left column of Fig. 4. At zero spacing, corresponding to $\eta = \xi = 0$, the correlation is perfect, i.e., has a value of unity. With increasing values of ξ and η, the value of R_ω drops rapidly and, for the case $\Delta^* = 0$, exhibits well-defined negative peaks along the η and ξ axes. The distance of these peaks from the origin is indicative of the vertical and horizontal spacing of the averaged vortical structures shown in Figs. 3a and 3b. At larger values of spacing between the plane of the laser sheet and the fin, corresponding to $\Delta^* = 0.06$, 0.12, and 0.18, similarly rapid drops of the magnitude of the correlation function R_ω occur near the origin $\xi = \eta = 0$. In these cases, there is no longer a single, well-defined negative peak for $\Delta^* = 0.06$ and 0.12, due to the more irregular forms of the corresponding averaged vorticity distributions in Figs. 3a and 3b.

Regarding the instantaneous distributions of the correlation functions, shown in the right column of Fig. 4, there are a large number of peaks over the ξ–η plane, corresponding to the multiple concentrations of positive and negative instantaneous vorticity in Figs. 3a and 3b. Since these concentrations are not spatially periodic, the peaks in the correlation function R_ω do not indicate spatial periodicity with increasing values of ξ and η. The interpretation of the instantaneous plot at $\Delta^* = 0$ is analogous to that of the averaged vorticity distribution shown in the foregoing. In this case, the instantaneous distributions of vorticity exhibit a nearly regular pattern (see lower left image of Fig. 3a); consequently, there is a single, well-defined negative correlation peak along the η axis and a positive one along the ξ axis, indicative of the spacing between vorticity concentrations. This pattern of concentrations becomes irregular at larger values of Δ^* shown in Figs. 3a and 3b and, correspondingly, the correlation plots at $\Delta^* = 0.06$–0.18 show decreasing regularity.

Nevertheless, there occur discernible peaks R_ω along the η and ξ axes, with the ones along the η axis being the most visible and indicating the preferred spacing between vortical structures.

V. Vorticity Fluctuations: Averaged Representations

The unsteady pressure on the surface of the fin is related to the fluctuating vorticity field adjacent to it. The power spectral density of the surface pressure, to be addressed subsequently, is an averaged representation of the pressure fluctuations. It is, therefore, appropriate to determine the averaged vorticity fluctuations, i.e., the root mean square of the vorticity fluctuations, as follows:

$$\tilde{\omega}_{\text{rms}} = \left\{ \frac{1}{N} \sum_{i=1}^{N} [\tilde{\omega}_i(x, y)]^2 \right\}^{\frac{1}{2}}$$

where $\tilde{\omega}_i(x, y)$ is the instantaneous vorticity fluctuation defined as $\tilde{\omega}_i(x, y) = \omega_i(x, y) - \bar{\omega}(x, y)$. Contours of constant $\tilde{\omega}_{\text{rms}}$ are illustrated in Fig. 5 for increasing distance Δ^* from the surface of the fin. Viewing all four images of Fig. 5, it is evident that the highest levels of $\tilde{\omega}_{\text{rms}}$ occur in the center of the broken-down vortex, just upstream of the leading edge of the fin, as indicated in the image at $\Delta^* = 0$. At $\Delta^* = 0.06$, slightly above the surface of the fin, relatively high levels of vorticity intersect the leading edge of the fin in the regions near the tip and near the root. At the other locations, especially over the surface of the fin, the levels of vorticity fluctuation are relatively low. The bold dots indicate locations of pressure taps. Considering the levels of fluctuating vorticity relative to the locations of the dots, it is anticipated that the largest pressure fluctuations will occur at the leading edge of the fin and lower fluctuations along its surface. In fact, this trend is exhibited by the pressure spectra of Sec. VI. At a larger distance from the surface of the fin, represented by $\Delta^* = 0.12$, the spatial variation of the vorticity levels is generally the same as

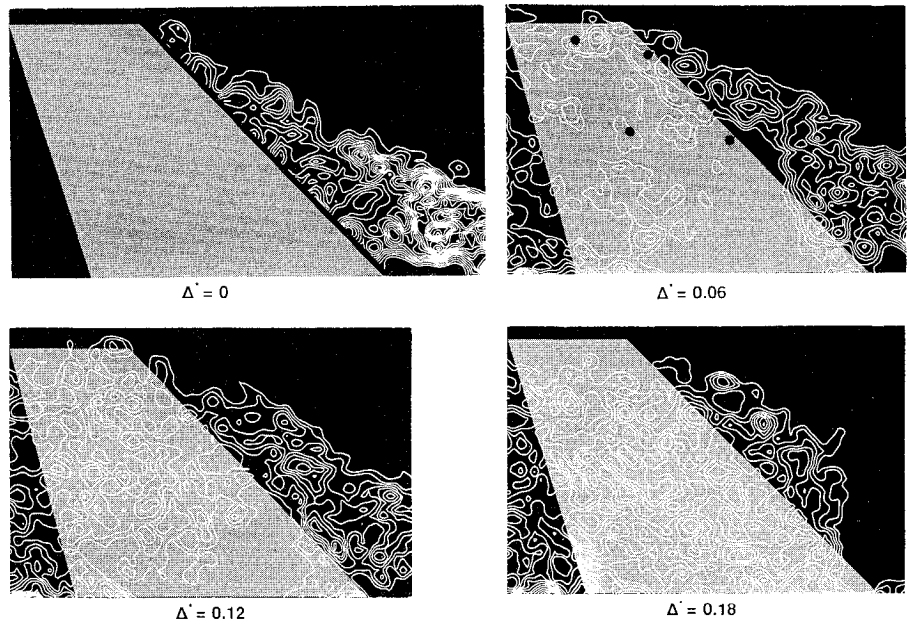

Fig. 5 Contours of constant root-mean-square fluctuating vorticity $\tilde{\omega}_{z_{\text{rms}}}$ on planes at increasing distance Δ^* from surface of fin; in all images, minimum and incremental values of $\tilde{\omega}_{z_{\text{rms}}}$ are 5 1/s and 1 1/s.

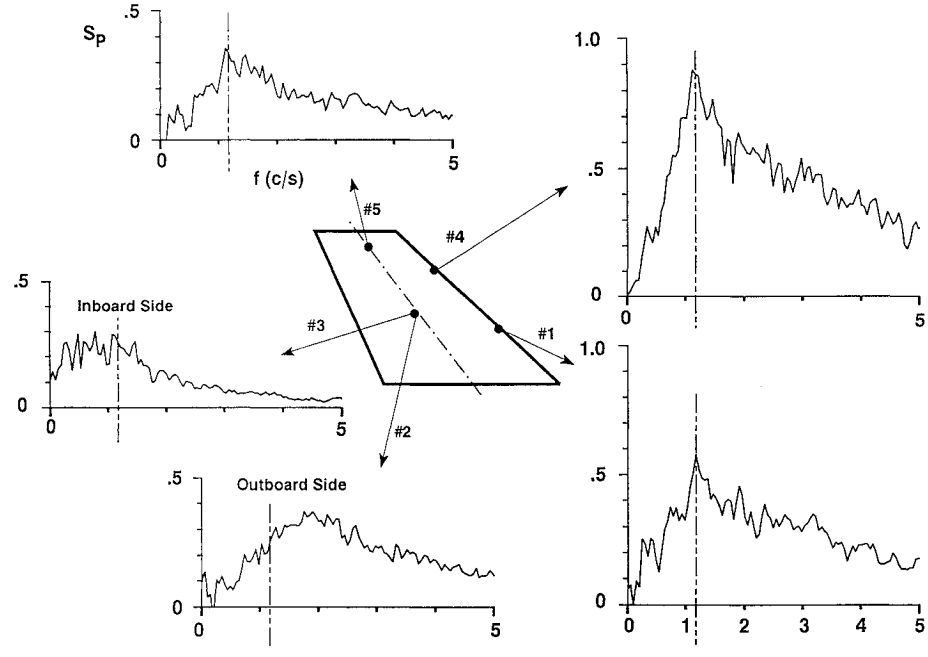

Fig. 6 Power spectral density of pressure fluctuations at indicated locations on surface of fin.

at $\Delta^* = 0.06$. Finally, at the largest distance $\Delta^* = 0.18$, substantial levels of vorticity still intersect the leading edge of the fin, but the region above it also exhibits significant values, most likely due to the outer edge of the large-scale separation zone on the outboard side of the fin.

VI. Spectra of Surface Pressure Fluctuations

The power spectral densities of the surface pressure at five locations on the surface of the fin are given in Fig. 6. For taps located along the leading edge and near the tip, the predominant peak of each spectrum occurs at approximately the same value of frequency $f = 1.2$ Hz. On the surface of the fin, the distribution of fluctuating energy is more broadly distributed and, on the outboard side, the predominant components are shifted to a higher value relative to those at the leading edge. This broader distribution of energy is associated with the distortion of the vorticity fields described in Fig. 3. The root mean square of the pressure fluctuation corresponds to the area under each of the spectral distributions of Fig. 6. The largest values of rms pressure correspond to the intersection of high levels of fluctuating vorticity with the leading edge of the fin, shown at $\Delta^* = 0.06$ in Fig. 5. Moreover, the lower values of rms pressure, which occur in the tip and central regions of the fin, correspond to regions of low fluctuating vorticity, evident in the image $\Delta^* = 0.06$ in Fig. 5. A detailed comparison of the spectra given in Fig. 6 with those of related investigations cited in Sec. I is given by Wolfe et al.[20]

VII. Concluding Remarks

Impingement of a broken-down vortex on a fin having a swept leading edge generates a complex flow structure associated with a large-scale separation zone extending over the surface of the fin. The principal features of this flow and the associated pressure fluctuations are as follows.

1) The instantaneous structure of the broken-down vortex upstream of the leading edge of the fin exhibits the classical staggered pattern of alternating positive and negative concentrations of vorticity. Along the leading edge of the fin, however, including the edge of the tip, negative concentrations of vorticity dominate; they are due to a separated mixing-layer flow along the edge of the fin.

2) Averaging of these instantaneous vorticity concentrations shows that a time-averaged, negative vorticity layer exists along the leading edge and tip of the fin.

3) Over the surface of the fin, the levels of fluctuating vorticity are significantly lower than those on the edge, at least in the region close to the fin surface. Correspondingly, averaged levels of vorticity are insignificant relative to those along the edge.

4) Root-mean-square levels of fluctuating vorticity, obtained from a large number of instantaneous images, show regions of low and high levels of $\tilde{\omega}_{\text{rms}}$ vorticity that are in good agreement with regions of low and high rms surface pressure.

5) Spectra of surface pressure fluctuations show peak values that, again, are well correlated with regions of high fluctuating vorticity. Although the frequency at which this peak occurs is unaltered in the leading-edge and tip region, there is substantial broadening and distortion of the energy content of the fluctuations in the central region of the fin. In this region, the instantaneous vorticity contours show both positive and negative contributions, appearing randomly from one instantaneous image to the next and having substantially lower levels than those negative contours along the edge of the fin.

Acknowledgments

The authors are pleased to acknowledge support of the Air Force Office of Scientific Research on Grants AFOSR-91-0055, F49620-93-1-0075, and F49620-94-1-0038.

References

[1]Triplett, W. E., "Pressure Measurements on Twin Vertical Tails in Buffeting Flow," *Journal of Aircraft*, Vol. 20, No. 11, 1983, pp. 920–925.

[2]Lee, B. H. K., Brown, D., Zgela, M., and Poirel, D., "Wind Tunnel Investigation and Flight Test of Tail Buffet on the F-18 Aircraft," AGARD CP 483, 1990, pp. 1-1–1-26.

[3]Brown, D., Lee, B. H. K., and Tang, F. C., "Some Characteristics and Effects of the F/A-18 LEX Vortices," *Vortex Flow Aerodynamics*, AGARD CP 494, 1990, pp. 30-1–30-20.

[4]Lee, B. H. K., and Tang, F. C., "Buffet Load Measurements on an F/A-18 Vertical Fin at High Angle-of-Attack," AIAA Paper 92-2127, Jan. 1992.

[5]Lee, B. H. K., and Brown, D., "Wind-Tunnel Studies of F/A-18 Tail Buffet," *Journal of Aircraft*, Vol. 29, No. 1, 1992, pp. 146–152.

[6]Lee, B. H. K., Brown, D., Tang, F. C., and Plosenski, M., "Flow Field in the Vicinity of an F/A-18 Vertical Fin at High-Angle-of-Attack," *Journal of Aircraft*, Vol. 30, No. 1, 1993, pp. 69–74.

[7]Ferman, N. A., Patel, S. R., Zimmerman, N. H., and Gerstenkorn, G., "A Unified Approach to Buffet Response of Fighter Aircraft Empennage," *AGARD/NATO 70th Structures and Materials Meeting* (Sorento, Italy), 1990, pp. 2-1–2-15.

[8]Shah, G. H., "Wind-Tunnel Investigation of Aerodynamic and Tail Buffet Characteristics of Leading-Edge Extension Modifications to the F/A-18," AIAA Paper 91-2889, Aug. 1991.

[9]Shah, G. H., Grafton, S. B., Guynan, N. D., Brandon, J. M., Dansberry, B. E., and Patel, S. R., "Effect of Vortex Flow Characteristics on Tail Buffet and High Angle of Attack Aerodynamics of a Twin-Tail Fighter Configuration," High Angle of Attack Technology Conf., NASA Langley Research Center, Hampton, VA, Oct.–Nov. 1990.

[10]Bean, D. E., and Wood, N., "An Experimental Investigation of Fin Buffeting and Suppression," AIAA Paper 93-0054, Jan. 1993.

[11]Washburn, A. E., Jenkins, L. M., and Ferman, M. A., "Experimental Investigation of Vortex-Fin Interaction," AIAA Paper 93-0050, Jan. 1993.

[12]Lee, J. W., Cavone, A. A., and Suzuki, K. E., "Doppler Global Velocimetry Measurements of the Vortical Flow Above an F-18," AIAA Paper 93-0414, Jan. 1993.

[13]Hebbar, S., Platzer, M., and Frink, W., Jr., "Vortex Wake Investigation of a Twin-Tail Fighter Aircraft Model at High Angles of Attack With and Without LEX Fences," AIAA Paper 93-0868, Jan. 1993.

[14]LeMay, S. P., and Lovato, J. A., "Experimental Investigation of the Vortex–Vertical Tail Interaction on an F-15," AIAA Paper 94-0070, Jan. 1994.

[15]Mayori, A., and Rockwell, D., "Interaction of a Streamline Vortex with a Thin Plate: A Source of Turbulent Buffeting," *AIAA Journal*, Vol. 32, No. 10, 1994, pp. 2022–2029.

[16]Rockwell, D., Magness, C., Robinson, O., Towfighi, J., Akin, O., Gu, W., and Corcoran, T., "Instantaneous Structure of Unsteady Separated Flows via Particle Image Velocimetry," Dept. of Mechanical Engineering and Mechanics, Lehigh Univ., PI-1 Rept., Bethlehem, PA, Feb. 1992.

[17]Rockwell, D., Magness, C., Towfighi, J., Akin, O., and Corcoran, T., "High-Image-Density PIV Using Laser Scanning Techniques," *Experiments in Fluids*, Vol. 14, 1993, pp. 181–192.

[18]Rockwell, D., and Lin, J.-C., "Quantitative Interpretation of Complex, Unsteady Flows via High-Image-Density Particle Image Velocimetry," SPIE International Symposium on Optics, Imaging and Instrumentation (San Diego, CA), Vol. 2005, Society of Photo-Optical Instrumentation Engineers, 1993, pp. 490–503.

[19]Fisher, D. R., Del Frate, J. H., and Zuniga, F. A., "Summary of In-Flight Flow Visualization Obtained from the NASA High Alpha Research Vehicle," NASA-TM-101734, Jan. 1991.

[20]Wolfe, S., Canbazoglu, S., Lin, J.-C., and Rockwell, D., "Buffeting of Fins: Assessment of Surface Pressure Loading," *AIAA Journal* (to be published).